

## REDSHIFT IN THE OPTICAL BAND GAP OF AMORPHOUS NANOSTRUCTURE $\text{Se}_{80}\text{Te}_{20-x}\text{Sn}_x$ FILMS

M. RASHAD<sup>a,b\*</sup>, R. AMIN<sup>c</sup>, M.M. HAFIZ<sup>a</sup>

<sup>a</sup>Physics Department, Faculty of Science, Assiut University, Assiut, Egypt.

<sup>b</sup>Physics Department, Faculty of Science, Tabuk University, P.O. Box 741, Tabuk, 71491, KSA.

<sup>c</sup>Physics Department, Faculty of Science, New Valley, Assiut University, Egypt.

Ternary glasses of  $\text{Se}_{80}\text{Te}_{20-x}\text{Sn}_x$  ( $x=3$  and 9 at.%) are prepared by melt quench technique. Thin films of  $\text{Se}_{80}\text{Te}_{20-x}\text{Sn}_x$  ( $x=3$  and 9 at.%) of different thicknesses in the range of (25 nm -1450 nm) are prepared by the conventional thermal evaporation technique on glass substrate. X-ray diffraction measurements show that both bulk and thin films of  $\text{Se}_{80}\text{Te}_{20-x}\text{Sn}_x$  have amorphous natures. Optical transmission and reflection spectra of the studied thin films are measured in the wavelength range of 200–2500 nm at room temperature. The absorption coefficient ( $\alpha$ ) as an optical constant is determined as a function of film thickness. The width of localized states near the mobility edge increases with increasing the film thickness. The optical band gap is redshifted from 1.87 to 1.49 eV and from 1.85 to 1.35 eV with increasing the film thickness for both  $\text{Se}_{80}\text{Te}_{20-x}\text{Sn}_x$  ( $x=3$  and 9 at.%) thin films respectively, due to quantum size effect.

(Received June 3, 2015; Accepted September 8, 2015)

*Keywords:* Chalcogenides; SeTeSn; Thin films, Optical constants.

### 1. Introduction

Chalcogenide glasses have been widely studied for their various and unique optical properties which make them very promising materials for use in optical and micro-optical elements such as gratings [1], optical recording media [2], fibre optics and waveguided devices in integrated optics since they exhibit a good transparency in the infrared region, especially at the telecommunication wavelengths at 1.30 and 1.55mm [3]. Characterization of linear optical properties of a material requires not only the values of both the refractive index and absorption coefficient at a specific wavelength but also the knowledge of their evolution as a function of the optical wavelength [4]. Various device applications like rectifiers, photocells, xerography, switching and memory, etc. have made selenium attractive. Unfortunately, pure Se element has disadvantages like short lifetime and low sensitivity. This problem can be overcome by alloying Se with some impurity atoms (As, Te, Bi, Ge, Ga, Sb etc), which gives higher sensitivity, higher crystallization temperature and smaller ageing effects [5-7]. Studying the effect of thickness on the optical gap provides a better understanding of the mechanism of disorder and defect formation in the chalcogenide films. The Se–Te alloys are found to be useful from the technological point of view if these alloys are thermally stable with time and temperature during use. However, thermal instability leading to crystallization is found to be one of the drawbacks of these alloys. Hence, attempts have been made to improve the stability of Se–Te by the addition of third element [8]. The insertion of an impurity e.g., Sb [9], Bi [10], Sn [11] in Se–Te binary alloy at the cost of Se is of interest owing to their various properties like higher glass transition temperature, higher crystallization temperature, and thermally more stable effects as compared to host Se–Te alloy. The addition of impurities like Sn is particularly of much interest as it has produced a remarkable change in the optical, electrical, and thermal properties of the chalcogenide glasses. Our group

---

\*Corresponding author: mohamed.ahemed24@science.au.edu.eg

have done the crystallization kinetics of this ternary glasses of  $\text{Se}_{80}\text{Te}_{20-x}\text{Sn}_x$  ( $x=3$  and 9 at.%) [12]. Therefore, in this work, the structural characteristics of amorphous  $\text{Se}_{80}\text{Te}_{20-x}\text{Sn}_x$  ( $x=3$  and 9 at.%) bulk and thin films are studied. Then the optical transmittance and reflectance spectra are analyzed to determine the optical constants for  $\text{Se}_{80}\text{Te}_{20-x}\text{Sn}_x$  ( $x=3$  and 9 at.%) thin films with different thickness ranged from 25 to 1450 nm.

## 2. Experimental

The bulk  $\text{Se}_{80}\text{Te}_{20-x}\text{Sn}_x$  ( $x=3$  and 9 at.%) chalcogenide glasses were prepared by the melt-quench technique. Materials (99.999% pure) were weighted according to their atomic percentages and were sealed in an evacuated silica tube, which was heated at 1100 °C for 15 h. The ampoule was frequently rocked at maximum temperature to make the melt homogeneous. The quenching was performed in ice water. Thin films were prepared by thermal evaporation at vacuum of  $10^{-5}$  Torr using an Edwards E-306 coating system. The evaporation rates as well as the film thickness were controlled by using a quartz crystal monitor, Edwards model FTMS.

The chemical composition of the samples was determined using the standard Energy Dispersive analysis of X-ray (EDX) technique, Jeol (JSM)-T200 type, Japan. The X-ray diffraction (XRD) of the as-prepared films was performed using Philips Diffractometer 1710 with Ni filtered Cu K $\alpha$  source ( $\lambda = 0.154$  nm). The transmittance ( $T$ ) and reflectance ( $R$ ) were recorded at room temperature using a double-beam spectrophotometer (Shimadzu UV-2101, Japan).

## 3. Results and discussion

### 3.1. Elemental analyses and XRD

Fig. 1 shows the EDX spectra of  $\text{Se}_{80}\text{Te}_{17}\text{Sn}_3$  and  $\text{Se}_{80}\text{Te}_{11}\text{Sn}_9$  thin films along with elemental percentage of different elements present in thin film. The inset figure 1 shows the EDX spectra of  $\text{Se}_{80}\text{Te}_{17}\text{Sn}_3$  and  $\text{Se}_{80}\text{Te}_{11}\text{Sn}_9$  bulk samples to compare with the thin film samples. The elemental percentage of these elements in thin film samples are nearly agreed with the starting bulk material. X-ray diffraction (XRD) measurements are performed in order to define the total phase nature of the as deposited thin films. Fig. 2 shows the XRD patterns of as-deposited  $\text{Se}_{80}\text{Te}_{17}\text{Sn}_3$  and  $\text{Se}_{80}\text{Te}_{11}\text{Sn}_9$  thin films. As illustrated from the figure, the absence of sharp diffraction peaks confirms the amorphous nature of these thin films.

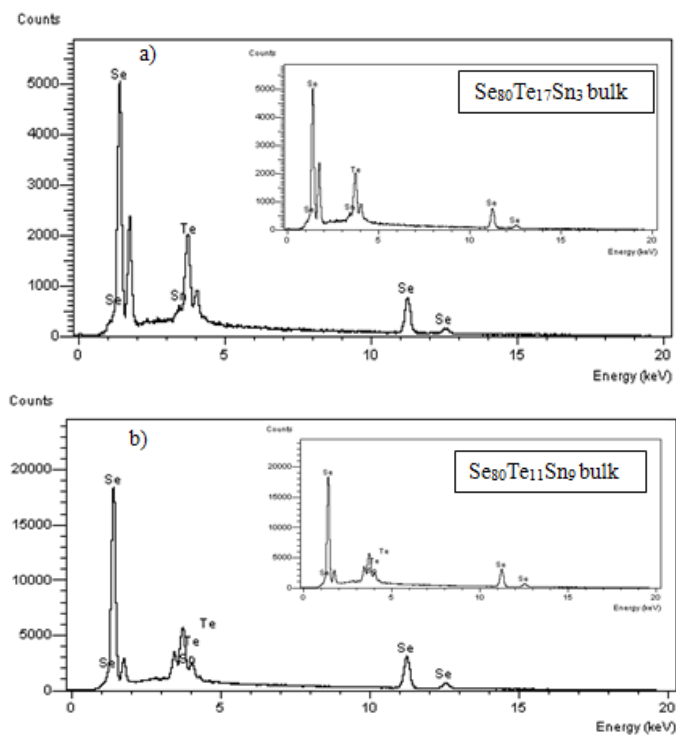


Fig. 1a: EDX of as-prepared  $Se_{80}Te_{17}Sn_3$  thin films of 1000 nm thick. (The inset figure is the EDX of  $Se_{80}Te_{17}Sn_3$  bulk samples). b: EDX of as-prepared  $Se_{80}Te_{11}Sn_9$  thin films of 1000 nm thick. (The inset figure is the EDX of  $Se_{80}Te_{11}Sn_9$  bulk samples).

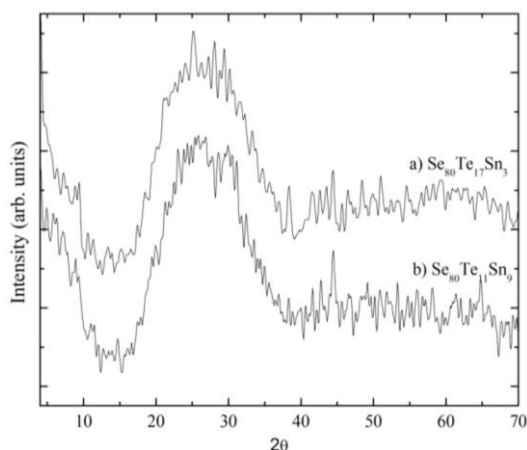


Fig. 2: X-ray diffraction patterns of as-prepared a)  $Se_{80}Te_{17}Sn_3$  and b)  $Se_{80}Te_{11}Sn_9$  thin films of 1000 nm thick.

### 3.1. Optical properties

The spectral distribution of the transmittance ( $T$ ) and reflectance ( $R$ ) of  $Se_{80}Te_{17}Sn_3$  and  $Se_{80}Te_{11}Sn_9$  films for different film thicknesses are shown in Figs. 3 and 4, respectively. In contrast to the reflectance, the transmittance increases as wavelength increases for all films. In addition, more interference peaks appear with increasing the film thickness. For wavelengths  $\lambda > 500$  nm, all films become transparent and neither light is scattered nor absorbed ( $R+T=1$ ), i.e., nonabsorbent region.

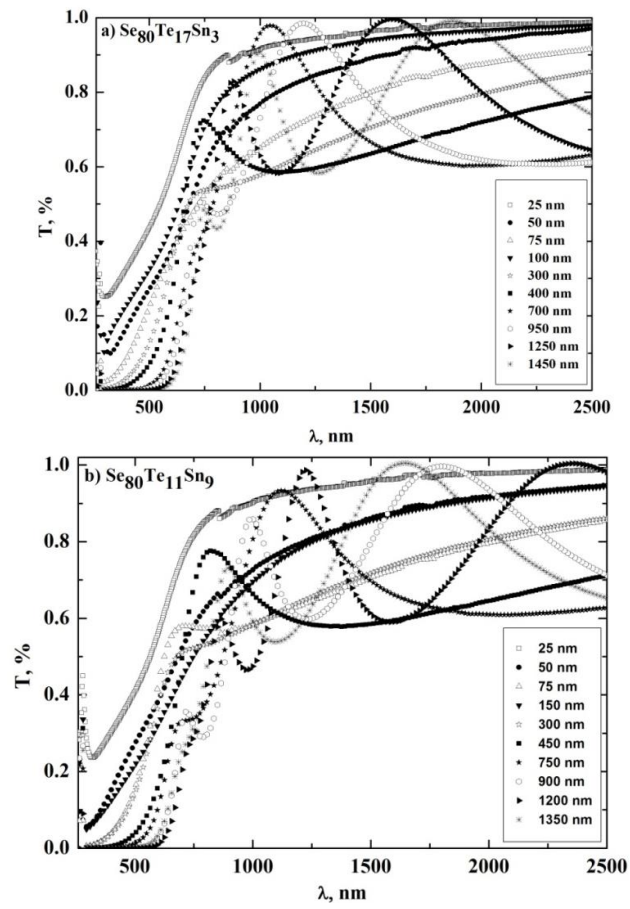


Fig. 3: Transmittance spectra ( $T$ ) of the a)  $\text{Se}_{80}\text{Te}_{17}\text{Sn}_3$  and b)  $\text{Se}_{80}\text{Te}_{11}\text{Sn}_9$  thin films of various thicknesses.

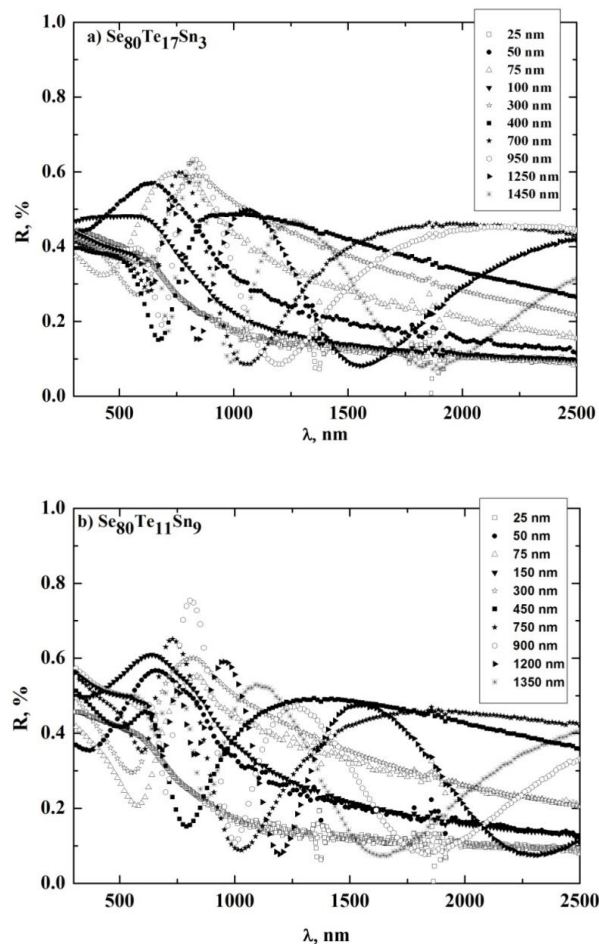


Fig. 4: Reflectance spectra ( $R$ ) of the a)  $Se_{80}Te_{17}Sn_3$  and b)  $Se_{80}Te_{11}Sn_9$  thin films of various thicknesses.

The absorption coefficient ( $\alpha$ ) was computed from the experimentally measured values of transmittance  $T(\lambda)$  and reflectance  $R(\lambda)$  according to the following relation [13]:

$$T = (1-R)^2 \exp(-\alpha d) / [1-R^2 \exp(-2\alpha d)] \quad (1)$$

where  $d$  (cm) is the film thickness. Fig. 5 shows the dependence of absorption coefficient ( $\alpha$ ) on the incident photon energy ( $h\nu$ ) for as-deposited  $Se_{80}Te_{17}Sn_3$  and  $Se_{80}Te_{11}Sn_9$  thin films with different film thicknesses. It is observed that the value of  $\alpha$  increases with increasing the photon energy. On the other hand, it decreases with increasing the film thickness.

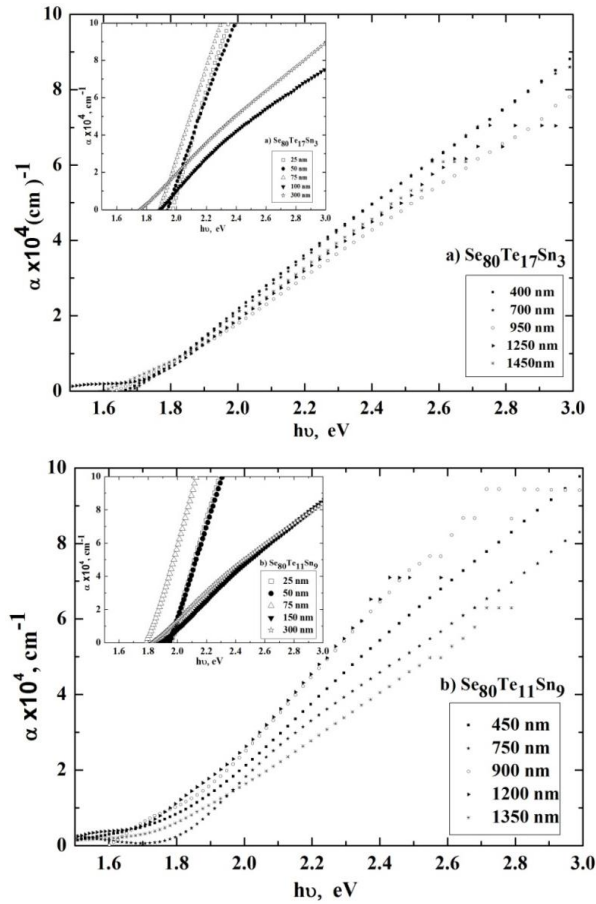


Fig. 5: Dependence of the absorption coefficient ( $\alpha$ ) on photon energy ( $h\nu$ ) for a)  $\text{Se}_{80}\text{Te}_{17}\text{Sn}_3$  and b)  $\text{Se}_{80}\text{Te}_{11}\text{Sn}_9$  thin films of various thicknesses. (The inset figure (a) is the dependence of absorption coefficient ( $\alpha$ ) on photon energy ( $h\nu$ ) for  $\text{Se}_{80}\text{Te}_{17}\text{Sn}_3$  at thicknesses of 25, 50, 75, 100 and 300 nm). (The inset figure (b) is the dependence of absorption coefficient ( $\alpha$ ) on photon energy ( $h\nu$ ) for  $\text{Se}_{80}\text{Te}_{11}\text{Sn}_9$  at thicknesses of 25, 50, 75, 150 and 300 nm).

As in all amorphous semiconductors [14-16], the spectral distributions of the absorption coefficient can be divided into three distinct regions. These are: a high absorption region is caused by band-to-band transition, an exponential edge region relates to the structural randomness of amorphous materials and a weak absorption tail that originates from the defects and impurities. For  $\alpha < 10^4 \text{ cm}^{-1}$ , there is usually an Urbach tail, where  $\alpha$  depends exponentially on the photon energy  $h\nu$  according to Urbach's empirical relation [17]:

$$\alpha(\nu) = \alpha_0 \exp(h\nu/E_e) \quad (2)$$

where  $\nu$  is the frequency of the incident light,  $\alpha_0$  is a constant and  $E_e$  is interpreted as the width of the tails of localized states in the gap region. In general,  $E_e$  represents the degree of disorder in an amorphous semiconductor. Fig. 6 shows the dependence of the natural logarithm of absorption coefficient on the photon energy for and  $\text{Se}_{80}\text{Te}_{17}\text{Sn}_3$  and  $\text{Se}_{80}\text{Te}_{11}\text{Sn}_9$  thin films with different film thickness. The reciprocal of the slope yields the magnitude of the width of the tail of localized states ( $E_e$ ) while the interception at lower energy gives  $\alpha_0$  according to Eq. (2). The values of  $E_e$  are strongly dependent on the film thickness as shown in Fig. 7. According to Mott and Davis [18], the width of localized states near the mobility edge depends on the degree of disorder and defects present in the amorphous structure. The dependence on the thickness of  $E_e$  can rise due to a large

density of structural defects (dislocations) as the thickness increases [19]. These defects can introduce localized states near the band edges resulting in an increase of  $E_e$ .

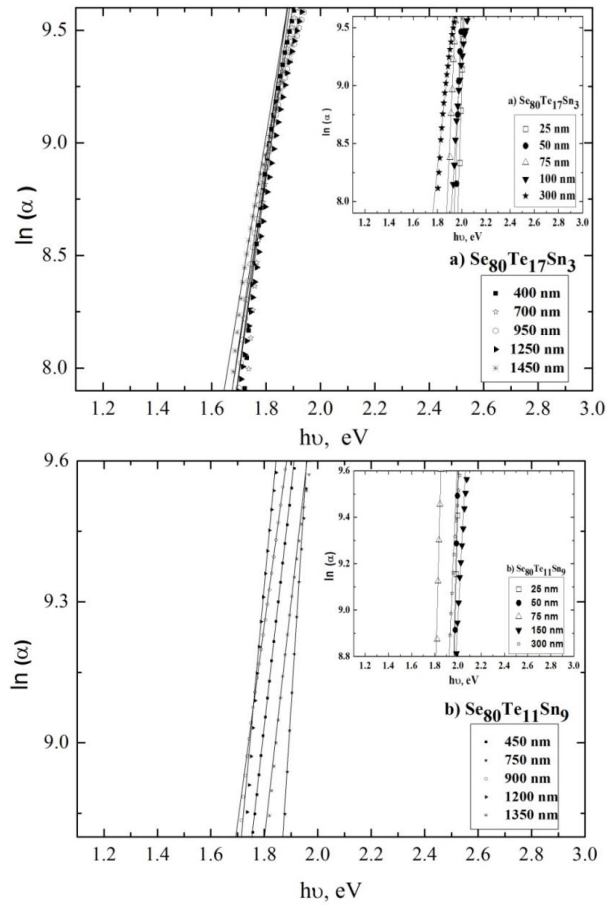


Fig. 6: Dependence of the  $\ln(\alpha)$  on photon energy ( $h\nu$ ) for a)  $\text{Se}_{80}\text{Te}_{17}\text{Sn}_3$  and b)  $\text{Se}_{80}\text{Te}_{11}\text{Sn}_9$  thin films of various thicknesses. (The inset figure (a) is the dependence of  $\ln(\alpha)$  on photon energy ( $h\nu$ ) for  $\text{Se}_{80}\text{Te}_{17}\text{Sn}_3$  at thicknesses of 25, 50, 75, 100 and 300 nm). (The inset figure (b) is the dependence of  $\ln(\alpha)$  on photon energy ( $h\nu$ ) for  $\text{Se}_{80}\text{Te}_{11}\text{Sn}_9$  at thicknesses of 25, 50, 75, 150 and 300 nm).

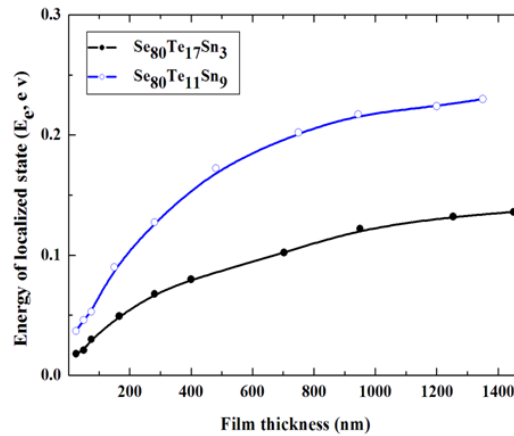


Fig. 7: The width of localized state tails ( $E_e$ ) of  $\text{Se}_{80}\text{Te}_{17}\text{Sn}_3$  and  $\text{Se}_{80}\text{Te}_{11}\text{Sn}_9$  thin films as a function of the film thickness.

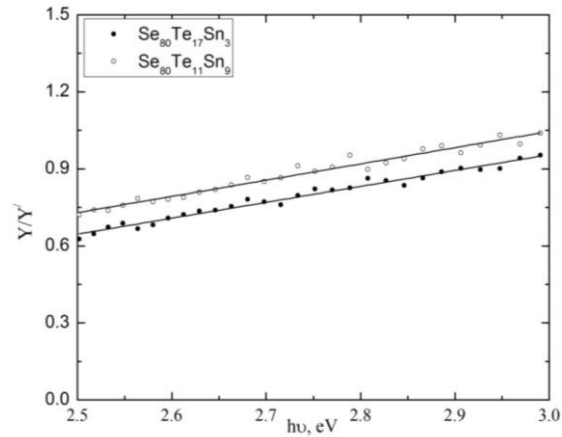


Fig. 8:  $Y/Y'$  of 300-nm thick  $Se_{80}Te_{17}Sn_3$  and  $Se_{80}Te_{11}Sn_9$  film.

For higher  $\alpha$  values of greater than  $10^{-4} \text{ cm}^{-1}$ ,  $\alpha$  takes the form [20, 21]:

$$\alpha h\nu = A(h\nu - E_g)^m. \quad (3)$$

Where  $E_g$  is the optical energy gap of the material and the exponent  $m$  characterizes the transitions process. The value of  $m$  is 2 for the indirect allowed transitions or  $1/2$  for direct allowed transition. Making the substitution that  $Y = \alpha h\nu$ , Eq. (3) can be written in the form [22]:

$$Y/Y' = (1/m) (h\nu - E_g), \quad (4)$$

where  $Y'$  is the derivative of  $Y$  with respect to photon energy ( $h\nu$ ). Eq. (4) is used to analyze the experimental data since it gives the ratio of  $Y/Y'$  as a linear function of ( $h\nu$ ) and offers a direct method for determining the exponent  $m$ . Fig. 8 displays the dependence of the ratio of  $Y/Y'$  on the photon energy for the  $Se_{80}Te_{17}Sn_3$  and  $Se_{80}Te_{11}Sn_9$  thin films. The best straight line is drawn through plotted points using the linear regression so the values of  $m$  are  $2 \pm 0.05$ . The value of  $m$  is closed to 2 indicating the electronic transition responsible for the photon absorption is non-direct process.

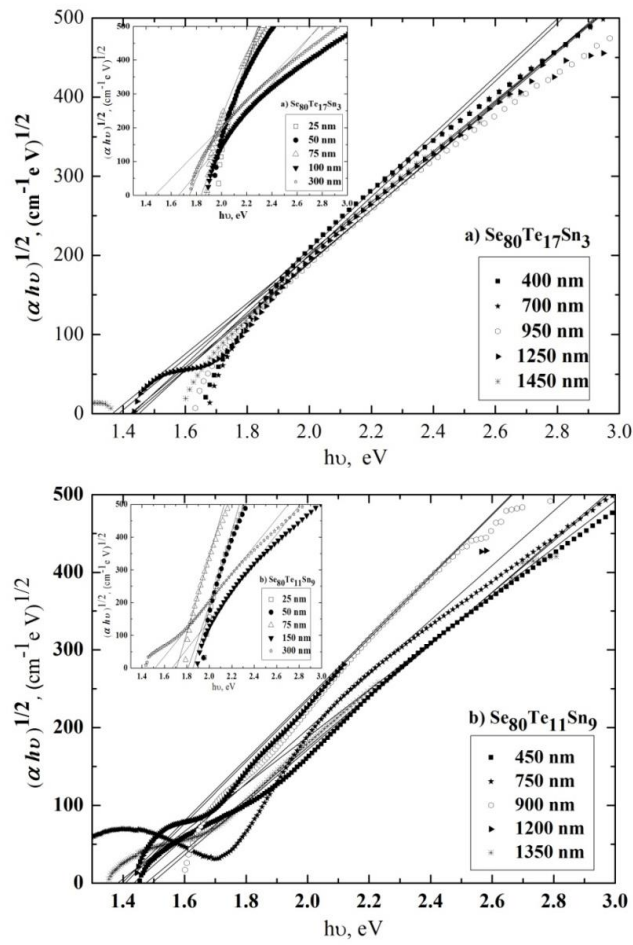


Fig. 9: variation  $(\alpha h\nu)^{1/2}$  as a function of photon energy ( $h\nu$ ) for a)  $\text{Se}_{80}\text{Te}_{17}\text{Sn}_3$  and b)  $\text{Se}_{80}\text{Te}_{11}\text{Sn}_9$  thin films of various thicknesses. (The inset figure (a) is  $(\alpha h\nu)^{1/2}$  for  $\text{Se}_{80}\text{Te}_{17}\text{Sn}_3$  at thicknesses of 25, 50, 75, 100 and 300 nm). (The inset figure (b) is  $(\alpha h\nu)^{1/2}$  for  $\text{Se}_{80}\text{Te}_{11}\text{Sn}_9$  at thicknesses of 25, 50, 75, 150 and 300 nm).

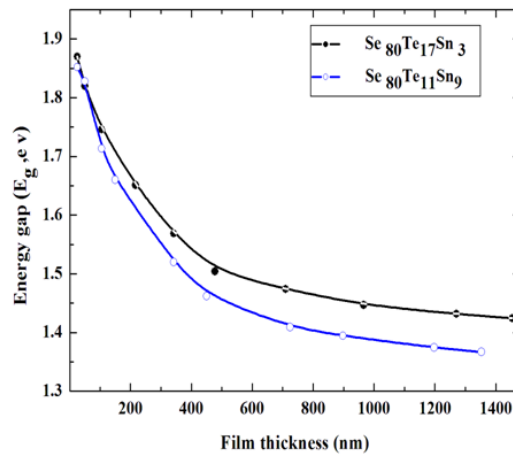


Fig. 10: Optical energy gap ( $E_g$ ) of  $\text{Se}_{80}\text{Te}_{17}\text{Sn}_3$  and  $\text{Se}_{80}\text{Te}_{11}\text{Sn}_9$  thin films as a function of the film thickness.

Fig. 9 shows linear  $(ah\nu)^{1/2}$  versus photon energy  $(h\nu)$  plots for the two films with different film thickness. Intercept of the straight line with the photon energy axis at  $(ah\nu)^{1/2} = 0$  gives the optical band gap,  $E_g$ . Fig 10 shows the thickness dependence of  $E_g$  for both  $\text{Se}_{80}\text{Te}_{17}\text{Sn}_3$  and  $\text{Se}_{80}\text{Te}_{11}\text{Sn}_9$  films.  $E_g$  decreases with increasing the film thickness. A similar behavior for  $E_g$  depending on the film thickness has been observed for  $\text{Ag}_2\text{Te}$  thin films [23]. This behavior can be explained in term of quantum size effect [24]. This behavior can be explained due to the defects present in the amorphous structure. On the other hand, this effect appears in semiconductors and semi-metal films when the thickness of the films is comparable with the mean free path and effective de-Broglie wavelength of the carriers. The transverse components of the electron states assume quasi-discrete energy values in thin films due to the finite size of the thickness. Accordingly, the bottom of the conduction and top of the valence band are separated by an additional amount  $\Delta E = h^2/8m^*d^2$  where  $d$  is the thickness of the film and  $m^*$  is the effective mass of the carrier. This means  $E_g$  is proportional to the square of reciprocal of thickness. Therefore, the decrease of  $E_g$  as film thickness increases is due to the quantization effect.

#### 4. Conclusion

Thin films of  $\text{Se}_{80}\text{Te}_{17}\text{Sn}_3$  and  $\text{Se}_{80}\text{Te}_{11}\text{Sn}_9$  with different thickness are amorphous materials as confirmed by the existence of a hump in the XRD patterns of the films. The results of EDX show that the elemental percentage of the composition elements of a specific film is nearly agreed with the starting bulk material. The optical absorption measurements for the as deposited  $\text{Se}_{80}\text{Te}_{17}\text{Sn}_3$  and  $\text{Se}_{80}\text{Te}_{11}\text{Sn}_9$  films indicate the indirect transition of the absorption mechanism. The width of localized states near the mobility edge increases with increasing the film thickness. The optical energy gap for the studied films is redshifted with increasing film thickness due to the energy quantization of the transverse components of the electron states.

#### References

- [1] J.M. Gonzalez-Leal, P. Krecmer, J. Prokop, S.R. Elliott, J. Non-Cryst. Solids **326–327**, 416 (2003).
- [2] T. Ohta, J. Optoelectron. Adv. Mater. **3**, 609 (2001).
- [3] T. Wagner, M. Krbal, J. Jedelsky, M. Vlcek, B. Frumarova, M. Frumar, J. Optoelectron. Adv. Mater. **7**, 153 (2005).
- [4] J. Liu, P. Taylor, Phys. Rev. B **41**, 3163 (1990).
- [5] A. A. Al-Ghamdi, Vacuum **80**, 400 (2006).
- [6] K. Shimakawa, J. Non-Cryst. Solids **77** (1985).
- [7] M. Saitar, J. Ledru A. Hamou, G. Saffarini, Physica B **248** (1998).
- [8] N.S. Saxen, J Non-Cryst Solids. **345** (2004).
- [9] E.R. Shaaban, I. Kansal, M. Shapaan, JMF. Ferreira, J. Therm Anal Calorim. **98**, 347 (2009).
- [10] A. Sharma, P.B. Barman, J Therm Anal Calorim. **96**, 413 (2009).
- [11] H. Kumar, N. Mehta, K. Singh, Phys Scr. **80**, 065602 (2009).
- [12] M. Rashad, R. Amin, M.M. Hafiz, Canadian Journal of Physics, **93** (8): 898-904 (2015).
- [13] M. Becker, H. Yfan, Phy. Rev. **76**, 1530 (1949).
- [14] R. J. Elliott and A. F. Gibson, An Introduction to Solid State Physics and Applications, El. B. Edition, McMillan (1982).
- [15] John M. Essick, Richard T. Mather, Am. J. Phys. **61** (1993).
- [16] J. Tauc, in Amorphous and Liquid Semiconductors Plenum Press, New York (1974).
- [17] F. Urbach, Phys. Rev. **92**, 1324 (1953).
- [18] N.F. Mott, E.A. Davis, Electronic Processes in Non-Crystalline Materials, Clarendon Press, Oxford (1979).
- [19] M. A. Mohammed, Eng. Technol. J. **27**, 1174 (2009).
- [20] J. Tauc, R. Grigorovici, A. Vancu, Phys. Stat. Solidi **15**, 627 (1966).
- [21] E. A. Davis, N.F. Mott, Philos. Mag. **22**, 903 (1970).

- [22] A. K. Ray and C. A. Hogarth, *J. Phys. D: Appl. Phys* **23**, 458 (1990).
- [23] M. Pandiaraman, N. Soundararajan, C. Vijayan, *J. Ovonic Res.* **7**, 21 (2011).
- [24] V. P. Bhatt, K. Gireesan, C.F. Desai, *Cryst. Res. Technol* **24**, 187 (1989).